Inversion of tracer test data using tomographic constraints

Niklas Linde,[1,2] Stefan Finsterle,[3] and Susan Hubbard[3]

Received 12 November 2004; revised 4 January 2006; accepted 23 January 2006; published 18 April 2006.

[1] We have developed a methodology for inverting tracer test data using zonation information obtained from two-dimensional radar tomograms to improve the (typically overly smooth) hydraulic conductivity fields obtained from conventional inversion of tracer test data. The method simultaneously yields two-dimensional estimates of hydraulic conductivity as well as petrophysical relationships that relate hydraulic conductivity to radar velocity; these relationships can be assumed to be stationary throughout the area of investigation or to vary as a function of zonation. Using a synthetic three-dimensional hydraulic conductivity field, we apply the developed inversion methodology and explore the impact of the strength and stationarity of the petrophysical relationship as well as the impact of errors that are often associated with radar data acquisition (such as unknown borehole deviation). We find that adding radar tomographic data to tracer test data improves hydrogeological site characterization, even in the presence of minor radar data errors. The results are contingent on the assumption that a relationship between radar velocity and hydraulic conductivity exists. Therefore the applicability of the proposed method may be limited to field sites where this condition is partially or fully satisfied.

Citation: Linde, N., S. Finsterle, and S. Hubbard (2006), Inversion of tracer test data using tomographic constraints, *Water Resour. Res.*, *42*, W04410, doi:10.1029/2004WR003806.

1. Introduction

[2] Hydrogeological variability exerts a major control on the movement of solutes in the subsurface. Spatial variability is often modeled using zonation [e.g., *Carrera and Neuman*, 1986a, 1986b, 1986c] or geostatistical approaches [e.g., *Hoeksema and Kitanidis*, 1984]. However, solving hydrogeological inverse problems using hydraulic head data only often leads to nonunique models, overly smooth models, or models where the zones are too large and the geometry of the zones has been arbitrarily defined, making it difficult to represent the underlying hydrogeological structure. *McLaughlin and Townley* [1996] note that a small number of other, complementary data (such as solute concentrations) might be more valuable than adding head measurements to an existing data set for the inverse problem of estimating a transmissivity field. Also, they state that geophysical methods offer attractive possibilities to supplement traditional hydrogeological data. *Scheibe and Chien* [2003] modeled the flow and transport of tracer test data from the fairly homogeneous Oyster site, Virginia, using different levels of conditioning data, including geophysical data. They show that hydraulic conductivity estimates conditioned to estimates of hydraulic conductivity provided by both radar tomograms and flowmeter data [*Hubbard et al.*, 2001] significantly improved transport predictions, compared to hydraulic conductivity estimates based on flowmeter data only.

[3] Although the potential benefits of including geophysical data in the estimation of hydrogeological properties have been demonstrated in recent years, many obstacles prohibit the routine use of geophysical data for quantitative hydrogeological estimation. While geophysical methods provide minimally invasive, densely sampled, and relatively inexpensive measurements, problems using geophysical data in hydrogeological parameter estimation often exist due to (1) a lack of direct and universal relationships between geophysical and hydrogeological properties, (2) spatially variable resolution of geophysical methods, (3) inversion artifacts caused by data acquisition errors, and (4) artificial smoothness of the geophysical tomograms caused by the regularization that is used to solve most geophysical inverse problems [e.g., *Day-Lewis and Lane*, 2004].

[4] Most high-resolution hydrogeological parameter estimation approaches that have been developed to date using geophysics have been carried out using cross-hole tomographic methods, including seismic [*Copty et al.*, 1993; *Hyndman et al.*, 1994], radar [*Chen et al.*, 2001; *Alumbaugh et al.*, 2002], and electrical resistance [*Daily et al.*, 1992]. Examples of hydrogeological parameter estimation using both geophysical and hydrogeological data include estimation of (1) the hydraulic conductivity and geometry of hydrofacies [*McKenna and Poeter*, 1995; *Hyndman and Gorelick*, 1996], where the geophysical data are used to delineate the geometry of hydrofacies; (2) smoothly varying hydraulic conductivity estimates [*Hubbard et al.*, 2001] and the spatial correlation of hydraulic conductivity [*Hubbard et al.*, 1999]; (3) sediment geochemistry [*Chen et al.*, 2004]; (4) moisture content [*Alumbaugh et al.*, 2002; *Binley et al.*,

[1]Department of Earth Sciences/Geophysics, Uppsala University, Uppsala, Sweden.
[2]Now at Centre Européen de Recherche et d'Enseignement des Géosciences de l'Environnement, CNRS, Université Paul Cézanne, Aix-en-Provence, France.
[3]Earth Sciences Division, Lawrence Berkeley National Laboratory, Berkeley, California, USA.

0043-1397/06/2004WR003806$09.00

2002]; (5) fracture geometry [*Slater et al.*, 1997]; and (6) solute transport monitoring [*Slater et al.*, 2002; *Day-Lewis et al.*, 2003].

[5] In many of these studies [e.g., *Chen et al.*, 2001; *Alumbaugh et al.*, 2002] the relationship between estimated geophysical parameters and hydrogeological properties is assumed to be stationary (i.e., constant within the study area), as well as independent of data acquisition errors and the inversion method used. In reality, these conditions are rarely met, for two reasons. First, petrophysical relationships may vary as a function of hydrogeological heterogeneity. For example, *Prasad* [2003] illustrated, using core data, how seemingly uncorrelated measurements of seismic velocity and hydraulic conductivity may have correlation coefficients as high as 0.9 if they are grouped into hydrogeologically similar units. This suggests that (1) the estimated petrophysical relationship may become unnecessarily weak if data from different hydrogeological units are grouped together in the estimation process, or (2) that a petrophysical relationship estimated using data from one type of hydrogeological unit might be invalid for other nearby units. Another complication is that the tomogram itself is an estimate rather than a precise image of geophysical properties. The tomogram is affected by many factors, including the aspect ratio of the distance between boreholes and the depth interval where measurements are carried out, data errors, the inversion method, and geological heterogeneity [e.g., *Peterson*, 2001; *Alumbaugh et al.*, 2002]. *Day-Lewis and Lane* [2004] suggest that the quantitative use of geophysical data for hydraulic parameter estimation can be challenging in the presence of such errors, even if a strong petrophysical relationship between radar velocity and a hydrogeological property exists.

[6] Recent research has focused on developing more robust approaches to develop field-scale petrophysical relationships using tomographic data. For example, *Moysey et al.* [2005] developed a framework to obtain field-scale estimates of petrophysical relationships given known petrophysical relationships at the core scale. With their approach, conditional realizations of the property of interest are generated using petrophysical relationships and geostatistical information. Hypothetical geophysical surveys and inversions of these realizations are subsequently performed. Thus an average or pixel-specific field-scale petrophysical relationship can be developed that takes scaling, measurement errors, and the inversion process into account. *Moysey et al.* [2005] applied their methodology to a synthetic case where radar traveltime data between boreholes and water saturation measurements in the vicinity of the boreholes were sampled. They report significant improvements in the estimates of water saturation between the boreholes compared with applying the petrophysical relationship at the core scale to the tomogram. However, a priori knowledge is needed about the spatial correlation structure of the property of interest, the errors of the data, and the petrophysical relationship at the core scale.

[7] To constrain the set of possible hydraulic conductivity fields in the vadose zone, *Kowalsky et al.* [2004] used time-lapse measurements of radar traveltimes and water saturation in hypothetical boreholes during a synthetic infiltration event. Instead of establishing a site-specific petrophysical relationship between hydraulic conductivity and radar velocity, a known petrophysical relationship between radar velocity and water saturation was utilized. *Kowalsky et al.* [2005] extended this work to estimate the petrophysical relationship as part of the inverse problem and successfully applied the method to data collected at the Hanford site in Washington.

[8] Rather than relying on a petrophysical relationship to map geophysical attributes associated with a tomogram to hydraulic property estimates, other studies have instead exploited the geometrical information offered by tomograms [*McKenna and Poeter*, 1995; *Hyndman and Harris*, 1996; *Eppstein and Dougherty*, 1998; *Tronicke et al.*, 2004]. *Hyndman et al.* [1994] jointly inverted two-dimensional synthetic seismic and tracer test data to estimate the geometry and hydraulic conductivity of hydrofacies, with the assumption that the geophysical variations delineate lithological zonation, which is in turn linked to hydraulic properties. *Hyndman and Gorelick* [1996] extended this approach to a three-dimensional analysis of three unique lithological classes. They applied their method to the Kesterson aquifer in California, where they obtained a reasonably good data fit to the tracer test data. The key assumption underlying the work by *Hyndman et al.* [1994] and *Hyndman and Gorelick* [1996] is that the individual zones have approximately constant hydrogeological and geophysical properties.

[9] *Hyndman et al.* [2000] established an a priori, linear, field-scale petrophysical relationship between seismic slowness estimates from tomograms and the logarithm of hydraulic conductivity using pump tests and core data at Kesterson, California, with a correlation coefficient of 0.74. In a later stage, they systematically perturbed the petrophysical relationship in order to estimate hydraulic conductivity fields that minimize the misfit of tracer and drawdown data. The tracer test data were better explained when the hydraulic conductivity realizations were conditioned to both hydraulic conductivity data and seismic tomograms compared with hydraulic conductivity data alone.

[10] Building on the work by *Hyndman et al.* [2000], we present a methodology to estimate hydraulic conductivity fields using radar tomograms without assuming that the petrophysical relationships are constant across interpreted velocity zones, and without assuming that the geophysical and hydrogeological properties are constant within the zones. The methodology can be applied to any data set that includes tracer data as well as geophysical tomograms generated by ray-based tomography. In this study, we focus on tomographic velocity estimates, inferred from cross-hole radar traveltime data. With our approach, each tomogram is automatically clustered into different zones based on the velocity variations. Each zone is assumed to have its own petrophysical relationship and the relationship does not need to be estimated a priori, but is instead estimated as part of the inversion. The inverse problem of estimating a hydraulic conductivity field is solved by zonewise estimation of the intercept and slope of the linear petrophysical relationship (which map the radar tomogram to the hydraulic conductivity field) by minimizing the misfit between observed and simulated tracer test data. The objective of this paper is threefold: (1) to present a new hydrogeophysical inverse methodology that uses velocity zonation from tomo-

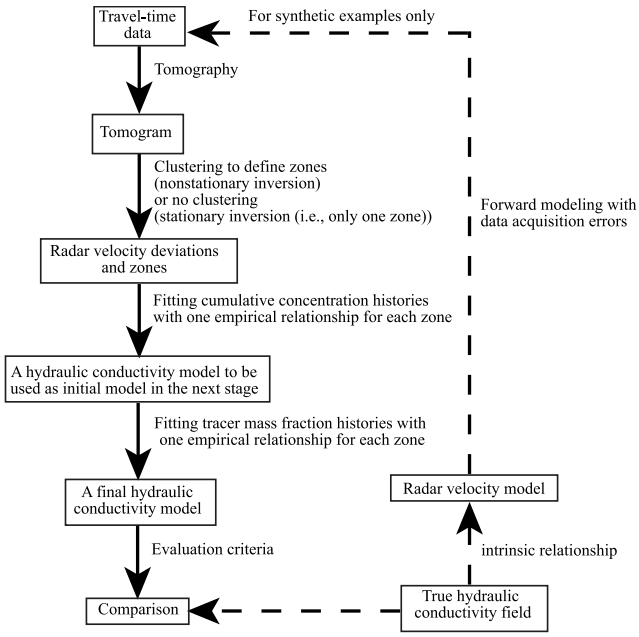

Figure 1. Flowchart of inversion methodology, where the true hydraulic conductivity field (lower right corner) is used to create synthetic data sets for the examples considered.

grams to constrain the inversion of tracer test data, (2) to use the developed methodology to explore how hydraulic conductivity estimates obtained using radar tomographic velocity information are influenced by radar data acquisition errors and assumptions about stationarity of the petrophysical relationship, and (3) to assess the benefits and limitations of incorporating tomographic information in the hydrogeological inversion for hydraulic conductivity even when the petrophysical relationship is weak or the radar data acquisition errors are significant.

[11] To address these objectives, we create a synthetic three-dimensional hydraulic conductivity field with characteristics similar to the Oyster site [*Hubbard et al.*, 2001]. We apply our methodology to a number of examples with different correlation coefficients between radar velocity and the logarithm of hydraulic conductivity, and consider the influence of various radar data acquisition errors on the inversion results.

[12] We demonstrate our proposed methodology using two-dimensional radar tomograms and three-dimensional flow and transport simulations, and summarize the benefits and difficulties of including geophysical data in the inversion of tracer test data. In section 2, we describe the inversion approach and define four evaluation criteria. In section 3, we present the results of the synthetic examples. Finally, in section 4 we discuss the results and present conclusions about the benefits and limitations of including tomographic data in estimating hydraulic conductivity fields using tracer test data.

2. Methodology

[13] In this section, we describe the general approach and assumptions behind our inversion methodology, present the types of radar and tracer data sets used in the inversion, and define four evaluation criteria to evaluate the inversion results.

[14] Let us define $Y = \log K$, where K (m/s) is the hydraulic conductivity, and log refers to a base of 10. We consider isotropic hydraulic conductivities, where $\boldsymbol{Y}$ indicates a three-dimensional array with all Y values in the discretized model volume (i.e., $\boldsymbol{Y}$ is not a hydraulic conductivity tensor) and $\hat{\boldsymbol{Y}}$ is the hydraulic conductivity estimate. Let $\boldsymbol{V}$ be a matrix that define the true radar velocity model and $\hat{\boldsymbol{V}}$ the corresponding tomogram obtained from inversion of radar traveltime data. Let $f(Y, V)$ denote the petrophysical relationship between Y and V, hereafter referred to as the intrinsic relationship, and $f(\hat{Y}, \hat{V})$ denote the petrophysical relationship between $\hat{Y}$ and $\hat{V}$, hereafter referred to as the empirical relationship. Let $\rho(Y, V)$ and $\rho(\hat{Y}, \hat{V})$ denote the correlation coefficients, hereafter referred to as the intrinsic correlation coefficient and empirical correlation coefficient, respectively.

[15] Our methodology is based on the following two key assumptions: (1) Major spatial variations in hydraulic conductivity are associated with spatial variations in the tomogram; however, spatial variations in the tomogram may not necessarily correspond to spatial variations in hydraulic conductivity. (2) Unknown stationary, linear empirical relationships between radar velocity and the logarithm of hydraulic conductivity are valid within specific zones of the tomogram. Relationships between radar velocity and the logarithm of hydraulic conductivity are site-specific and, even if a strong and linear petrophysical relationship exists at one site [*Chen et al.*, 2001], relationships at other sites are essentially unknown.

[16] The inversion is performed in the following steps. First, we perform an inversion of the geophysical data. Second, we define velocity zones within the tomogram. Third, we fit tracer test data by estimating a hydraulic conductivity field by zonewise estimation of the intercept and slope of the linear petrophysical relationships used to map the tomogram onto a hydraulic conductivity estimate. Finally, we evaluate the hydraulic conductivity estimate. A schematic flowchart is provided in Figure 1; a detailed description follows below.

2.1. Tomographic Zones

[17] In this study, we explore the utility of synthetic high-resolution radar traveltime data for constraining the tracer test inversion. The radar velocity contrasts considered in our examples are on the order of 10%; the straight ray approximation is therefore valid [*Peterson*, 1986; *Gritto et al.*, 2004]. We use the algebraic reconstruction technique (ART) for the tomographic inversion [*Peterson et al.*, 1985], which was the method used to invert the Oyster data [*Hubbard et al.*, 2001] on which we base our synthetic examples in section 3. More elaborate inversion methods exist (such as simultaneous iterative reconstruction technique (SIRT) or a regularized least squares solution using LSQR [*Paige and Saunders*, 1982]), but for the small velocity contrasts that we explored here (which are typical for semiconsolidated to unconsolidated sediments common in environmental investigations), the quality of the tomogram is mainly determined by the data and the survey geometry (J. Peterson, personal communication, 2004).

[18] We discretize the tomograms into uniform pixels (0.3×0.3 m^2), somewhat finer compared to the expected

resolution, which varies within the tomogram as a function of survey design [e.g., *Rector and Washbourne*, 1994; *Schuster*, 1996]. For the inversion, we use the traveltime associated with the difference between the first-arrival energy and the "zero time," which is the time associated with signal initiation. The ART algorithm does not provide a stopping criterion for the inversion. High-quality radar data allow many iterations for a given damping parameter to fit progressively finer features of the data. However, for noisy data, too many iterations will fit the noise and thereby introduce inversion artifacts. While the optimal number of iterations is unknown in real applications, the number of iterations is not so significant as long as it is reasonably close to the optimal number [*Peterson*, 1986]. In this synthetic study, our final tomogram is the tomogram that minimizes a L_1 norm, Φ_V, of the deviations between the true and the estimated velocity tomogram

$$\Phi_V = \sum_{i=1}^{NZ} \sum_{j=1}^{NX} \left| V_{ij} - \hat{V}_{ij} \right| \Delta_{ij}, \tag{1}$$

where NZ and NX are the number of pixels in the z (vertical) and x (horizontal) direction of the tomogram, respectively, and Δ_{ij} is 1 if the relative ray intensity for the corresponding pixel is above a certain threshold value; otherwise it is 0. The relative ray intensity is defined as the number of rays passing a pixel, normalized by the number of rays that pass the most densely covered pixel. Note that $\boldsymbol{V}$ is unknown in real applications, where the common stopping criterion is to iteratively seek a solution until the forward response of the model fits the observed data within the estimated errors. The resulting models are "best case" models because the optimal number of iterations is used. However, in the synthetic examples presented below we investigate the inherent information loss related to the tomography and specific data acquisition errors, such as deviated boreholes, errors that are also unknown in real applications.

[19] A radar tomogram typically has a number of zones in which the radar velocity is distinctly different from that in surrounding areas. These zones might correspond to different lithological zones and be associated with different intrinsic relationships, which we aim to estimate in the subsequent hydrogeological inversion (see section 2.3). We use the following automated clustering method to divide the tomogram into different zones.

[20] 1. Calculate the median, $\hat{V}_{med}$, of the tomogram.

[21] 2. Assign +1 and −1 to all tomographic pixels that are above or below the median, respectively, and that have a relative ray intensity above a threshold value of 0.25.

[22] 3. Cluster the pixels into different zones u, such that no pixel has a neighboring pixel with the same type (+1 or −1) that does not belong to the same zone, and such that each pixel is defined to have eight neighboring pixels (except at the boundaries).

[23] 4. Discard zones that consist of just a few pixels (in our study less than seven).

[24] 5. For each pixel, calculate the deviation from the median.

[25] Zones with few cells are discarded to keep the number of model parameters small, and because such zones are likely to have an insignificant impact on flow and transport. The corresponding pixels are treated as the background field together with areas where the relative ray intensity is low. Other criteria besides deviations from the median are necessary in certain cases (e.g., the presence of a trend in the tomogram) and more elaborate clustering techniques, such as k means clustering could be used, a method in which pixels are iteratively regrouped into a predefined number of clusters until the variability of the values within each group is minimized [*Tronicke et al.*, 2004]. Step 2 in our clustering method must be modified when using tomograms that do not use ray-based tomography. The threshold value in Step 2 could be defined by calculating the model resolution matrix [*Menke*, 1984] and by defining a cutoff related to the best resolved areas. In real applications, the resulting zonation patterns depend on the number of iterations if using the ART algorithm or on the regularization and the estimated data errors if a regularized least squares solution is sought. The differences in the zonation patterns occur in areas where the deviation from the median is low; such pixels get hydraulic conductivity values close to the background hydraulic conductivity when applying our hydrogeological inversion regardless of which zone the pixel belongs to (see section 2.3).

[26] A different approach to zonation not examined in this work is to define the zones as a part of the inverse problem [e.g., *Hyndman and Harris*, 1996; *Eppstein and Dougherty*, 1998]. Such a data-driven approach to zonation is preferable when zonation implies that the geophysical properties are constant with each zone. However, our zonation only implies that petrophysical relationships are constant within each zone.

[27] We also consider the case in which all pixels with a relative ray intensity above the threshold belong to a single zone, thereby assuming that the empirical relationship is constant throughout the tomogram.

[28] The next step is to carry out the hydrogeological inversion to estimate, for each zone, the empirical relationship that transforms the tomogram into a hydraulic conductivity estimate that minimizes the misfit between observed and simulated tracer test data.

2.2. Tracer Test Data

[29] The tomographic zones are used to constrain the set of possible hydraulic conductivity fields when inverting tracer test data. The data vector, $\boldsymbol{d}$, in the hydrogeological inverse problem is defined as

$$\boldsymbol{d} = \left[X_{11}^{obs}, \ldots, X_{P1}^{obs}, \ldots, X_{pn}^{obs}, \ldots, X_{PN}^{obs} \right], \tag{2}$$

where x_{pn}^{obs} is an observed tracer mass fraction at sampling location p at the nth observation time. Unfortunately, it is not practical to use tracer mass fractions in the initial iterations of the hydrogeological inversion. The initial hydraulic conductivity estimate must be close to the true field for local optimization methods to reach a global minimum using tracer breakthrough curves. The problem arises because each data point is considered to be an independent measurement (i.e., it is possible to locally improve the data fit by for example fitting the front of the observed breakthrough curve with the tail of the simulated breakthrough curve). Therefore we use a two-step hydrogeologic inversion methodology, outlined below, in which

the first step aims at finding a better initial hydraulic conductivity estimate to fit the tracer breakthrough data. In the second step, the tracer mass fraction data are matched directly (see equation (2)).

[30] The first step of the hydrogeological inversion involves fitting an approximation of the integrals

$$\int_{t_0}^{t_n} X_p dt \tag{3}$$

at different times t_n and sampling locations p, where t_0 is the time of tracer injection. We use a linear interpolation of equation (3):

$$\Psi_{pn}^{obs} = \sum_{i=1}^{n} \left(\frac{X_{pi}^{obs} + X_{p(i-1)}^{obs}}{2} \right) (t_i - t_{i-1}), \tag{4}$$

where Ψ_{pn}^{obs} is referred to as the observed cumulative concentration history, and t_i is the time of the ith observation. The simulated cumulative concentration history, Ψ_{pn}^{sim}, is defined in a similar fashion. This representation is an integrative measure that distinguishes between early and late arrivals. The same objective could be achieved by fitting the traveltimes for different percentiles.

[31] We assume for simplicity that the errors in the observed tracer mass fractions are normally distributed with zero mean and a standard deviation s. An estimate of the standard deviation for the cumulative concentration history, s_{pn}^{cum}, is

$$s_{pn}^{cum} = \sqrt{\sum_{i=1}^{n} (t_i - t_{i-1})} s. \tag{5}$$

We justify this measure by the fact that the accumulation of uncorrelated zero-mean Gaussian errors can be considered a random walk, and the distance from the origin of a random walk has an expected value of the square root of the sum of the individual steps [*Spitzer*, 1976].

2.3. Model Parameters and Inversion Methodology

[32] In this section, we define the model vector, $\boldsymbol{m}$, used in the hydrogeological inversion, as

$$\boldsymbol{m} = \left[Y_b, \beta_1, \ldots, \beta_u, \ldots, \beta_U, l_1, \ldots, l_p, \ldots, l_P \right], \tag{6}$$

where Y_b is a background hydraulic conductivity from which we calculate deviations; β_u is the slope of the empirical relationship in the uth zone (determined using the clustering method in section 2.1); and l_p is the logarithm of the loss factor (see below) at the pth sampling location. We seek two-dimensional hydraulic conductivity models because the radar tomograms used in the subsequent examples are two-dimensional. However, the observed tracer mass fraction moves through a heterogeneous three-dimensional hydraulic conductivity field. A large fraction of the tracer moves out of the plane between the boreholes (i.e., the area sampled by the radar survey) and will not be recovered in the boreholes where the tracer is sampled. The loss factors represent the fraction of observed tracer that reaches the samplers compared with the amount of simulated tracer that reaches the samplers using the estimated models with two-dimensional heterogeneity. A loss factor of one indicates that heterogeneity perpendicular to the radar tomogram is negligible and a loss factor of zero indicates that out-of-plane heterogeneity controls tracer transport. Accordingly, the simulated tracer mass fraction, $\hat{X}_{pn}^{sim}$, at sampling location p and observation time n is transformed to

$$\hat{X}_{pn}^{sim\prime} = 10^{l_p} \hat{X}_{pn}^{sim}, \tag{7}$$

where $\hat{X}_{pn}^{sim\prime}$ is the transformed simulated tracer mass fraction, which is compared with the observed tracer mass fraction; the transformed simulated cumulative concentration histories are calculated in an analogous way.

[33] Hydraulic conductivities are calculated by

$$\hat{Y}_{ij} = Y_b + \beta_{\Gamma_{ij}} \left(\hat{V}_{ij} - \hat{V}_{med} \right), \tag{8}$$

where Γ_{ij} is an integer that identifies the estimated zone u for pixel ij. The estimated hydraulic conductivity at pixel ij equals the background hydraulic conductivity if $\beta_{\Gamma ij}$ is 0.

[34] The hydrogeological inversion is carried out using iTOUGH2 [*Finsterle*, 1999], which we have modified to accommodate the calculation of the cumulative concentration histories (equation (4)) and the hydraulic conductivity representation (equation (8)). The hydrogeological forward model is based on TOUGH2 [*Pruess et al.*, 1999]. The inverse problem is solved by minimizing the following two objective functions:

$$\Phi_{cum} = \sqrt{\frac{1}{PN} \sum_{i=1}^{P} \sum_{j=1}^{N} \left(\frac{\Psi_{pn}^{sim\prime} - \Psi_{pn}^{obs}}{S_{pn}^{1/2}} \right)^2}, \tag{9}$$

is minimized during the first step of the inversion, and

$$\Phi_{conc} = \sqrt{\frac{1}{PN} \sum_{i=1}^{P} \sum_{j=1}^{N} \left(\frac{X_{pn}^{sim\prime} - X_{pn}^{obs}}{W_{pn}^{1/2}} \right)^2}, \tag{10}$$

during the second step, where $\boldsymbol{S}$ and $\boldsymbol{W}$ are diagonal matrices that contain the estimated error variances, $(s_{pn}^{cum})^2$ (see equation (5)) and s^2, respectively. Our resultant hydraulic conductivity estimate from the first step of the inversion is used as an initial estimate in the second step, where we fit the tracer mass fraction data (see equation (2)). The Levenberg-Marquardt algorithm [*Marquardt*, 1963] is used to minimize the objective functions, where the Jacobian is calculated with forward finite difference quotients for the first few iterations and central finite difference quotients for the last few iterations. The inversion ends when the decrease of the objective function is less than one percent between iterations; approximately 10 iterations are needed for the examples presented in section 3.

2.4. Definition of Evaluation Criteria

[35] We define a set of evaluation criteria to facilitate comparisons between different hydraulic conductivity estimates obtained through application of the developed inversion approach on the synthetic examples presented in section 3. The first criterion is the objective function (criterion 1), defined by equation (10). However, because

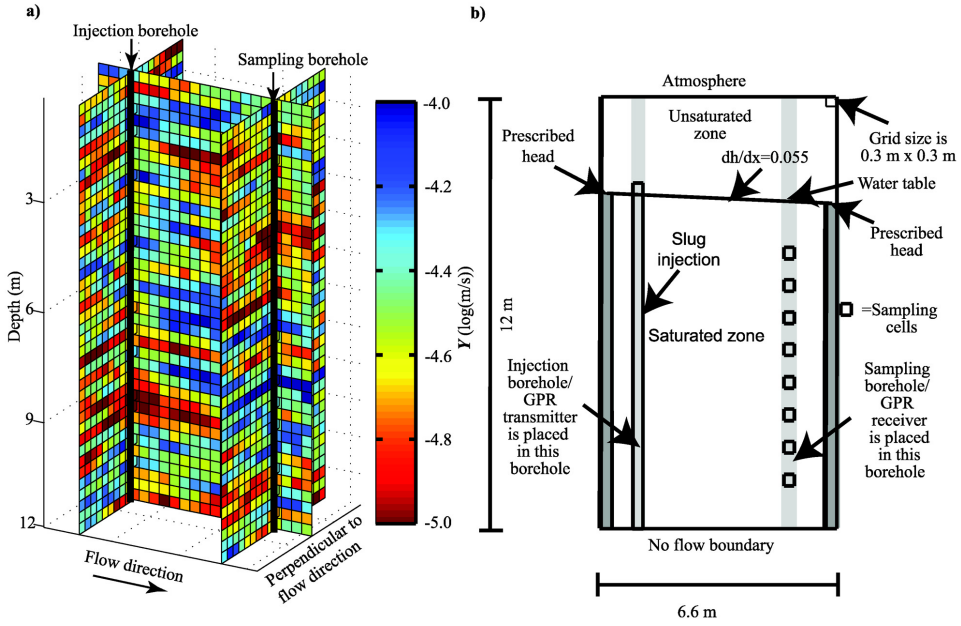

Figure 2. (a) True hydraulic conductivity field ***Y***. (b) Test layout.

there is an infinite set of hydraulic conductivity models that equally well can explain the observed tracer mass fractions, data fit is an insufficient measure. The empirical correlation coefficient between the estimated and true hydraulic conductivities, $\rho(\hat{Y}, Y)$ (criterion 2), is calculated for the pixels where the relative ray intensities are above the threshold value. Criterion 2 evaluates the trends in the hydraulic conductivity estimates compared to the true hydraulic conductivity field. The geometric mean of the hydraulic conductivity field is calculated as a measure of the effective hydraulic conductivity. As a performance criterion, we calculate $Y_{eff} - \hat{Y}_{eff}$ (criterion 3). Criterion 3 tests whether the estimate is unbiased. Lastly, we estimate the slope of the empirical relationship between the estimated radar velocities and the logarithm of estimated hydraulic conductivities, $\hat{\beta}$(μs/m) (criterion 4), using a least squares solution for the pixels above the relative ray intensity threshold.

3. Synthetic Examples

[36] In this section, we apply our hydrogeological inversion method to estimate hydraulic conductivity fields using tracer breakthrough data for a set of synthetic examples, where radar velocity tomograms are used to constrain the inverse problem. We assess the influence of different intrinsic relationships and geophysical data acquisition errors on the resulting hydraulic conductivity estimates.

[37] We first generate the true three-dimensional hydraulic conductivity field using an unconditional sequential Gaussian simulation [*Deutsch and Journel*, 1998] with an exponential variogram model and a spatial correlation structure similar to that at the Oyster site [*Hubbard et al.*, 2001]. An exponential semivariogram model with integral scales of I_x = 1.5 m, I_y = 1.5 m, and I_z = 0.3 m, and a standard deviation of σ_Y = 0.26 (see Figure 2a) are used. The intrinsic relationship is defined by scaling the generated hydraulic conductivity field such that the lowest hydraulic conductivity corresponds to a radar velocity of 58 m/μs and the highest value to 64 m/μs, which is the range of radar velocity values observed at the Oyster site [*Hubbard et al.*, 2001]. The resulting intrinsic relationship is $Y = -18.73 + 0.2323 \times V$, where V is given in m/μs. The intrinsic relationship is used to map the true hydraulic conductivity field (Figure 2a) onto the true velocity model.

[38] We also want to apply the methodology to synthetic examples where the intrinsic correlation coefficient is not perfect (i.e., the correlation coefficient is not one). This is accomplished by creating a set of radar velocity models, $\boldsymbol{V_k}$, that have different intrinsic correlation coefficients, but have the same standard deviation and integral scales as the true radar velocity model. We do this by generating a new hydraulic conductivity field, $\boldsymbol{Y_0}$, that has the same standard deviation and integral scales as the true hydraulic conductivity field but no correlation with the true hydraulic conductivity field (i.e., the correlation coefficient is zero). These two hydraulic conductivity fields allow us to calculate a set of hydraulic conductivity fields that have intermediate correlation coefficients with the true field, as follows:

$$\boldsymbol{Y_k} = \boldsymbol{Y_0} + k(\boldsymbol{Y} - \boldsymbol{Y_0}), \tag{11}$$

where k = 0.5 in the example presented in section 3.3. We use the intrinsic relationship to map the hydraulic conductivity field onto a velocity model, $\boldsymbol{V_k}$.

[39] We simulate cross-hole radar tomographic surveys using the different velocity models and by incorporating different data acquisition "errors". For the simulations we used a multioffset gather (MOG) survey, in which transmitters and receivers have a spacing of 0.3 m along the borehole between the water table and the no-flow boundary (refer to Figure 2b). This survey layout resulted in 450 model parameters (30 × 15 pixels with a size of 0.3 × 0.3 m^2). We restrict the inversions of the radar data to rays with angles less than 45°, because high-angle raypaths traveling through the earth are often difficult to

distinguish from faster rays traveling within the boreholes [*Peterson*, 2001] and because most inversion algorithms assume that radar antennas act like a point source, thereby overestimating velocities when inverting data with high angular coverage [*Irving and Knight*, 2005]. The survey layout gives 628 traveltimes from low-angle raypaths, which were used in the subsequent ART inversion. We considered errors caused by (1) incorrect assumptions regarding the zero times (0.33 ns, 1 ns), (2) random errors in the horizontal position of the individual transmitters and receivers (taken from a uniform distribution with values between −2 cm and 2 cm), (3) inaccurate depth information (−5 cm) and horizontal separation between boreholes (−10 cm), and (4) boreholes assumed to be vertical are in fact deviated by 2% of depth. The errors are chosen to represent typical errors that are often encountered during radar surveys (J. Peterson, personal communication, 2004). In real applications, the sample rate of the waveforms is typically 0.4 ns giving a maximum picking error of less than 0.2 ns, which is considered to be insignificant, and thus picking is neglected herein as a potential source of error. We assume that we can accurately distinguish between direct waves and critically refracted waves from the water table [*Rucker and Ferré*, 2004]. In practice, it is often necessary to perform the inversion with measurements starting at least 0.25–0.5 m below the water table. The data are inverted using the ART technique, as described in section 2.1. We use the resulting tomogram to estimate the zones using the approach described in section 2.1. Note that fewer zones are estimated when we consider realistic data acquisition errors, because the L_1 norm defined in equation (1) is minimized after a few iterations (see discussion about ART inversion in section 2.1). Hence resolving fewer features leads to fewer zones.

[40] The observed tracer data are obtained by simulating flow and transport through the true three-dimensional hydraulic conductivity field (Figure 2a) from a 9.3 m line source using a slug injection of 280 g of bromide (Figure 2b), assuming a constant effective porosity of 30%, and neglecting dispersion within the pixels. The bromide concentration is synthetically sampled with multilevel samplers every 0.9 m in depth at one vertical borehole every 18 hours over 19 days, with an error of 100 ppb, which is a typical error in field investigations.

[41] The two-step hydrogeological inversion described in sections 2.2 and 2.3 is carried out. To test the potential of estimating different empirical relationships in different zones, the breakthrough curves are inverted twice for each example, (1) by estimating an empirical relationship for each zone, and (2) by estimating a single empirical relationship for the entire model domain. We use the terms ''nonstationary'' and ''stationary'' inversion to refer to these two types of inversions, respectively.

[42] Below, we visually describe and evaluate five examples of how the hydraulic conductivity estimates obtained using tracer and radar data are affected by (1) the ART inversion (example 1; section 3.1); (2) nonstationary intrinsic relationships (example 2; section 3.2); (3) weak intrinsic relationships (example 3; section 3.3); (4) geophysical data acquisition errors (but no errors caused by unknown borehole deviations) (example 4; section 3.4); and (5) errors caused by unknown borehole deviations (example 5; section 3.5). The five examples are defined in Table 1; a comparison of the evaluation criteria score (refer to section 2.4) of all examples are discussed in section 3.6.

3.1. Example 1: Benefits of Including "Ideal" Tomographic Data in the Hydrogeological Inversion

[43] We consider an example in which the intrinsic relationship is stationary, the intrinsic correlation coefficient is high (0.99), and the radar data acquisition errors are very small (see example 1 in Table 1). This example illustrates the loss of resolution inherent in radar inversion and its consequences for the hydrogeological inversion.

[44] The tomogram (Figure 3b) is a smooth estimate of the true radar velocity model (Figure 3a). It captures the major features in the central part of the model area, but is less accurate in the upper and lower parts, as well as close to the boreholes. The zonation pattern based on the clustering algorithm described in section 2.1 is shown in Figure 3c. The hydraulic conductivity estimates inferred from the nonstationary inversion (Figure 3e) and the stationary inversion (Figure 3f) contain the main features of the true hydraulic conductivity field (Figure 3d). Note that the nonstationary inversion is poor in resolving low conductivity zones because the tracer bypasses such zones through more conductive zones that are out of the plane defined by the tomogram. The nonstationary inversion is more sensitive to three-dimensional heterogeneity than the stationary inversion because it can estimate different empirical relationships in different zones; therefore the estimates based on the nonstationary inversion provide an effective hydraulic conductivity for the regions sampled by the tracer, whereas the estimates based on the stationary inversion are localized to variations along the tomogram. The corresponding histograms (Figure 3h Figure 3i) show that the residuals are largest in the nonstationary inversion. Scatterplots of the true hydraulic conductivity field against the nonstationary (Figure 3k) and the stationary (Figure 3l) hydraulic conductivity estimates show a strong correlation between the hydraulic conductivity estimates and the true hydraulic conductivity field, with correlation coefficients of 0.64 and 0.85, respectively. The slopes of the empirical relationships (0.19 μs/m and 0.31 μs/m) are rather close to the slope of the intrinsic relationship (0.23 μs/m). We can conclude that both the nonstationary and stationary inversions work satisfactorily for this example, but that the stationary inversion is superior when the intrinsic relationship is stationary.

[45] To illustrate the value of including tomograms to constrain the set of possible inverse solutions, we perform an inversion of the tracer test data only (referred to as example 0 in Table 1) and compare the results with those obtained above using both tracer test data and a tomogram. The zonation pattern was obtained by interpolating hypothetical flowmeter data in the boreholes using simple kriging with the integral scales used to generate the true hydraulic conductivity field (i.e., I_x = 1.5 m, I_y = 1.5 m, and I_z = 0.3 m). The clustering algorithm described in section 2.1 was carried out on the kriged field and it was assumed that the hydraulic conductivity within each of the resulting nine zones was constant (Figure 3g). This zonation approximates a possible zonation based on interpolation of geological or geophysical logs (e.g., gamma logs) between boreholes. Note that the kriged estimate of the flowmeter data is used to get the zonation only, i.e., the resulting

Table 1. Definition of Synthetic Examples and the Criteria Scores of the Resulting Models[a]

Definition of Examples and Criteria Scores	Example										
	0	1_{NS}[b]	1_{S}[b]	2_{NS}[c]	2_{S}[c]	3_{NS}[d]	3_{S}[d]	4_{NS}[e]	4_{S}[e]	5_{NS}[f]	5_{S}[f]
Definition of examples											
k[g]	does not apply	0.9	0.9	0.9	0.9	0.5	0.5	0.9	0.9	0.9	0.9
$\rho(Y, V)$	does not apply	0.99	0.99	0.99	0.99	0.57	0.57	0.99	0.99	0.99	0.99
Random deviation (2 cm)	does not apply	2	2	2	2	2	2	2	2	2	2
Vertical offset, cm	does not apply	0	0	0	0	0	0	−5	−5	0	0
Horizontal offset, cm	does not apply	0	0	0	0	0	0	−10	−10	0	0
Error in zero time, ns	does not apply	0.33	0.33	0.33	0.33	0.33	0.33	1.0	1.0	0.33	0.33
Deviation from vertical of right borehole, %	does not apply	0	0	0	0	0	0	0	0	2	2
Different intrinsic relationships	does not apply	no	no	yes	yes	no	no	no	no	no	no
Different empirical relationships	does not apply	yes	no	yes	no	yes	no	yes	no	yes	no
Tracer test data only	yes	no	no	no	no	no	no	no	no	no	no
Criteria scores											
Cr1: Φ_{conc}	6.4	5.6	7.9	5.9	21.8	4.5	14	10.3	9.7	11	13
Cr2: $\rho(Y, \hat{Y})$	0.094	0.64	0.85	0.75	0.53	0.42	0.64	0.72	0.80	0.36	0.45
Cr3: $Y_{eff} - \hat{Y}_{eff}$	−0.27	−0.064	−0.023	−0.031	−0.031	−0.099	−0.017	−0.038	−0.023	−0.036	−0.059
Cr4: $\hat{\beta}$, μs/m	does not apply	0.19	0.31	does not apply	does not apply	0.18	0.26	0.33	0.41	0.053	0.11

[a]Example 0 corresponds to the example where only tracer test data were used, whereas examples 1–5 used zonation from radar tomograms (subscript NS denotes nonstationary inversion, and subscript S denotes stationary inversion). The rows specify the values of k (see equation (11)), the intrinsic correlation coefficient, the random horizontal errors of the transmitters and receivers within the boreholes, the error in the depth information of the receivers, errors in the horizontal separation of the boreholes, errors in the zero times, percent deviation from vertical in one of the boreholes, if different intrinsic relationships were used in the zones, if different empirical relationships were used in the inversion, and if only tracer test data were used. The last four rows specify the scores of the evaluation criteria: Cr1 (objective function), Cr2 (correlation coefficient between true and estimated hydraulic conductivity field), Cr3 (difference between the geometric means of the true and estimated hydraulic conductivity field), and Cr4 (slope of the empirical relationship, the intrinsic relationship is 0.2323 m/μs).

[b]Section 3.1.

[c]Section 3.2.

[d]Section 3.3.

[e]Section 3.4.

[f]Section 3.5.

[g]See equation (11).

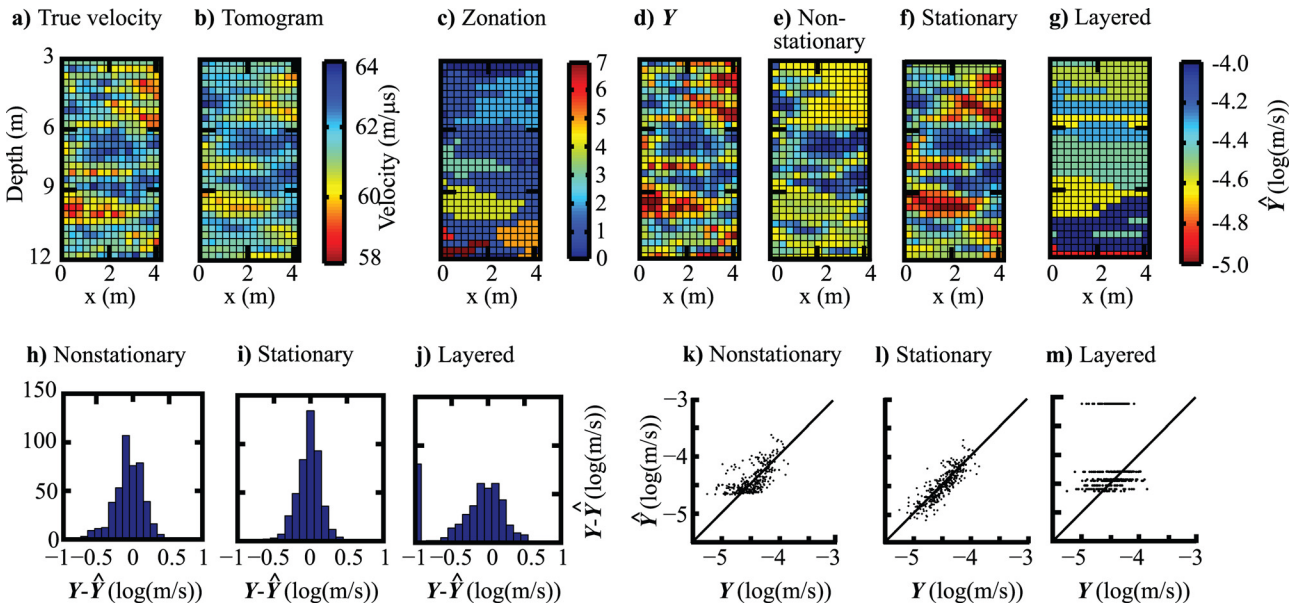

Figure 3. Results from example 1 where data acquisition errors are small, the intrinsic correlation coefficient is 0.99, and the intrinsic relationship is stationary (see example 1 in Table 1). (a) True velocity model, (b) tomogram, (c) tomographic zones used in the nonstationary inversion, (d) true hydraulic conductivity field, (e) hydraulic conductivity estimate from nonstationary inversion, (f) hydraulic conductivity estimate from stationary inversion, (g) hydraulic conductivity estimate when neglecting tomogram, (h) histogram of the residual of true and estimated hydraulic conductivity field from nonstationary inversion, (i) histogram of residuals of true and estimated hydraulic conductivity field from stationary inversion, (j) histogram of residuals of true and estimated hydraulic conductivity field when neglecting tomogram, (k) scatterplot of true and estimated hydraulic conductivity field from nonstationary inversion, (l) scatterplot of true and estimated hydraulic conductivity field from stationary inversion, and (m) scatterplot of true and estimated hydraulic conductivity field when neglecting tomogram.

models are not conditioned to any known hydraulic conductivity values. Despite the relatively large number of layers considered, the resulting variability in the hydraulic conductivity distribution is low (Figure 3g), except for one zone at the bottom of the model where the hydraulic conductivity is severely overestimated (this parameter is poorly constrained by the inversion), and the residuals (Figure 3j) are therefore larger compared with the inversions that have been regularized by the tomograms. The scatterplot (Figure 3m) shows a low correlation coefficient of 0.094. This comparison demonstrates the importance of accurately regionalizing the subsurface to avoid estimation bias, as reflected by the low variability in the hydraulic conductivity field obtained with the zoned model parameterization. The objective function (5.6 for the nonstationary inversion, 7.9 for the stationary inversion, and 6.4 for the inversion that did not utilize the tomograms) is an insufficient measure of model performance, because the more satisfying model (judged from criterion 2) from the stationary inversion has a slightly higher objective function compared to the inversion that did not utilize the tomogram in constraining the inversion.

[46] This example illustrates the improvement in the estimation of the hydraulic conductivity distribution obtained by regularizing the hydrogeological inverse problem using tomograms, seen most clearly by comparing the scatterplots (see Figures 3k–3m).

3.2. Example 2: Influence of Nonstationary Intrinsic Relationships

[47] The nonstationary inversion can potentially handle different intrinsic relationships in different zones. This situation might exist, for example, in heterogeneous subsurface regions that have dramatically different lithofacies. To illustrate that different petrophysical relationships can be handled, we use the example discussed in section 3.1, but reflect the hydraulic conductivity values of Zone 4 (Figure 4c) around the median (Figure 4d), making the originally low-hydraulic-conductivity zone hydraulically more conductive (see example 2 in Table 1). The true velocity model (Figure 4a), the tomogram (Figure 4b), and the zonation pattern (Figure 4c) are the same as in the previous example.

[48] The nonstationary hydraulic conductivity estimate (Figure 4e) contains the main features of the true hydraulic conductivity field, including the new hydraulically conductive zone. The estimate based on the stationary inversion (Figure 4f) results in a very smooth model. This is illustrated in the corresponding histograms (Figures 4g and 4h). The scatterplot of the nonstationary inversion estimate (Figure 4i) is comparable with the previous example (correlation coefficient of 0.75), whereas the scatterplot of the stationary inversion estimate (Figure 4j) reveals a much lower correlation coefficient of 0.53. The resulting hydraulic conductivity estimates are more strongly correlated to the true hydraulic conductivity field compared with the hydrau-

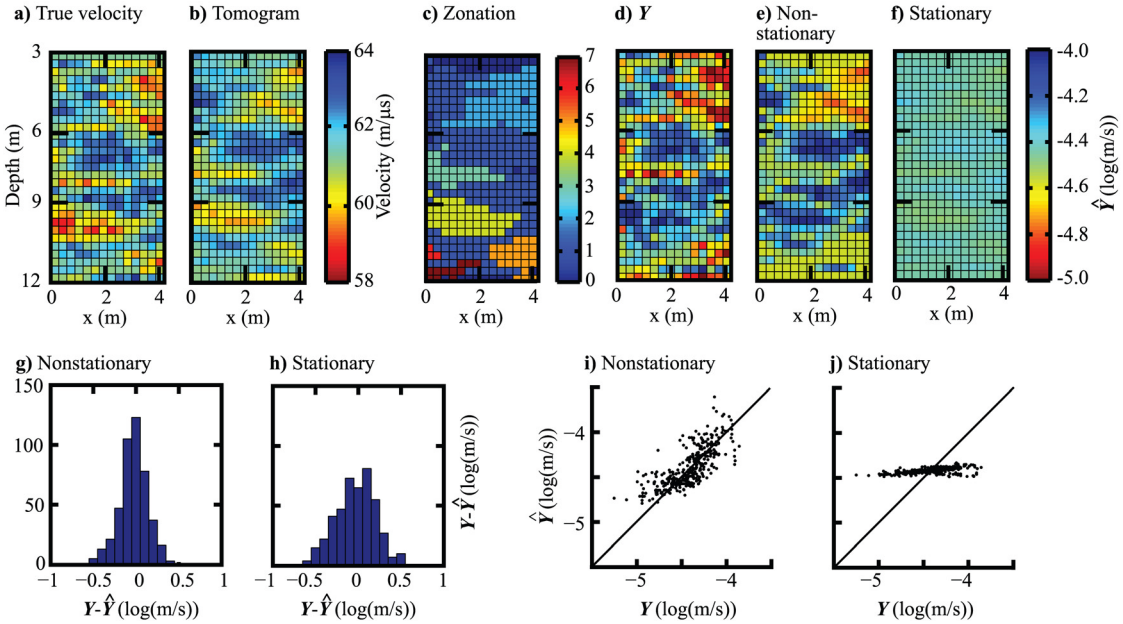

Figure 4. Results from example 2 where data acquisition errors are small, the intrinsic correlation coefficient is 0.99, and the intrinsic relationship is nonstationary (example 2 in Table 1). (a) True velocity model, (b) tomogram, (c) tomographic zones used in the nonstationary inversion, (d) true hydraulic conductivity field, (e) hydraulic conductivity estimate from nonstationary inversion, (f) hydraulic conductivity estimate from stationary inversion, (g) histograms of residuals of true and estimated hydraulic conductivity field from nonstationary inversion, (h) histograms of residuals of true and estimated hydraulic conductivity field from stationary inversion, (i) scatterplot of true and estimated hydraulic conductivity field from nonstationary inversion, and (j) scatterplot of true and estimated hydraulic conductivity field from stationary inversion.

lic conductivity estimate based on tracer test data only (see Figure 3g, correlation coefficient of 0.094).

[49] For this example, we conclude that the nonstationary inversion can handle different intrinsic relationships (see Figure 4i), and that the stationary inversion is unable to provide a reasonable model (see Figure 4j) and provides a very smooth model. The stationary inversion fails because the assumption of a single petrophysical relationship uniformly applied through the model domain is invalid.

3.3. Example 3: Weak Intrinsic Relationship

[50] In this example, we consider a more realistic, i.e., weaker correlation between radar velocity and hydraulic conductivity. Although there is no universal relationship between radar velocity and hydraulic conductivity [e.g., *Annan*, 2005] nor between seismic velocity and hydraulic conductivity [*Pride*, 2005], site-specific relationships may exist at some sites. The effective dielectric constant is linearly related to the inverse of the electrical formation factor [e.g., *Lesmes and Friedman*, 2005], which is a measure of the effective interconnected porosity [e.g., *Revil and Cathles*, 1999], thereby providing a possible link between radar velocity and hydraulic conductivity. *Chen et al.* [2001] found that radar velocity estimates inferred from radar tomography correlated reasonably well (with a correlation coefficient of 0.68) with collocated estimates of the logarithm of hydraulic conductivity inferred from flowmeter data at the South Oyster Site, VA, and other examples provided in section 1 described the use of seismic velocities for estimating hydraulic conductivity. Nevertheless, the correlation between the geophysical attributes and hydraulic conductivity is site-specific and may not exist for some sites, and the applicability of the method presented herein to real field data has yet to be demonstrated. In this example of a rather weak intrinsic relationship, we use $V_{0.5}$ (correlation coefficient 0.57; Figure 5a) as the velocity model from which we calculate the radar traveltime data (see example 3 in Table 1). The resulting tomogram and zonation pattern are shown in Figures 5b and 5c, respectively.

[51] The resulting hydraulic conductivity estimates (Figure 5e and Figure 5f) are distorted (Figure 5g and 5h) compared with the true hydraulic conductivity field (Figure 5d). In particular, the nonstationary inversion yields hydraulic conductivity estimates that are too conductive (refer to Figure 5i). The correlation coefficients between the true and estimated hydraulic conductivity for the nonstationary and stationary inversions are 0.42 and 0.64, respectively.

[52] We conclude that in the presence of weak intrinsic relationships, the stationary inversion provides hydraulic conductivity estimates that better reflect the true hydraulic conductivity field than the estimates based on the nonstationary inversion. Furthermore, even when there is only a weak and stationary petrophysical relationship, the zonation information provided by the tomographic data can be used to improve the estimation of hydraulic conductivity over the estimates obtained using tracer test data only (see Figure 3g, correlation coefficient of 0.094).

3.4. Example 4: Effects of Radar Data Acquisition Errors

[53] In this example, we consider the influence of radar data acquisition errors on the estimates of hydraulic con-

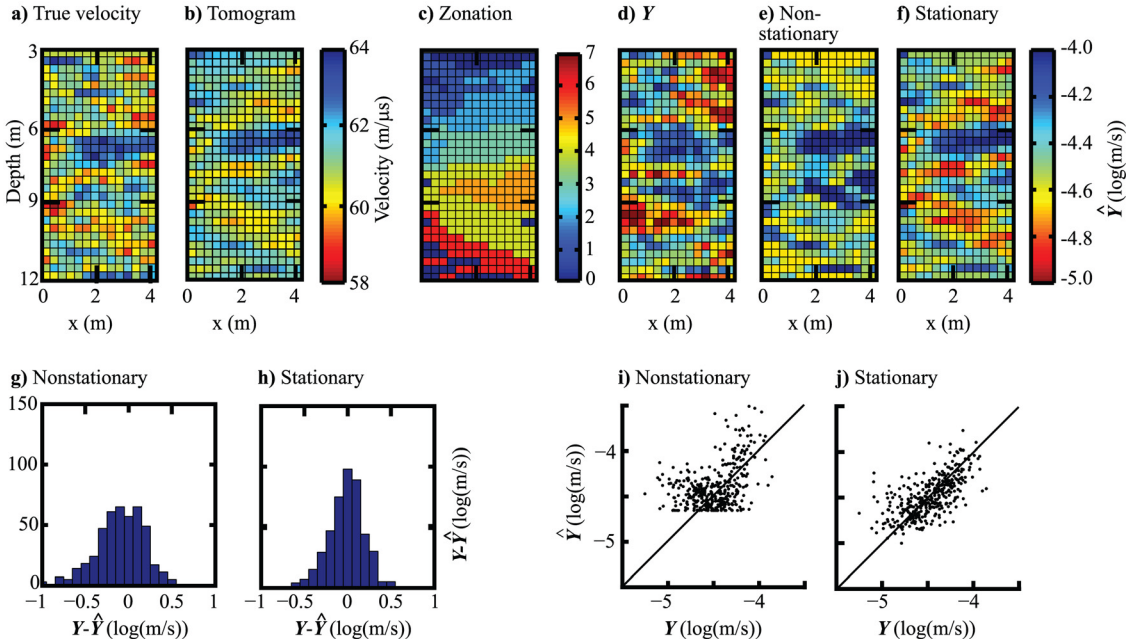

Figure 5. Results from example 3 where data acquisition errors are small, the intrinsic correlation coefficient is 0.57, and the intrinsic relationship is stationary (example 3 in Table 1). (a) True velocity model, (b) tomogram, (c) tomographic zones used in the nonstationary inversion, (d) true hydraulic conductivity field, (e) hydraulic conductivity estimate from nonstationary inversion, (f) hydraulic conductivity estimate from stationary inversion, (g) histogram of residuals of true and estimated hydraulic conductivity field from nonstationary inversion, (h) histogram of residuals of true and estimated hydraulic conductivity field from stationary inversion, (i) scatterplot of true and estimated hydraulic conductivity field from nonstationary inversion, and (j) scatterplot of true and estimated hydraulic conductivity field from stationary inversion.

ductivity. To simulate typical data acquisition errors, we have artificially increased the zero time error to 1 ns, incorporated a 5 cm error in the depth of the receivers, and reduced the assumed distance between the boreholes by 10 cm (i.e., example 4 in Table 1). The resulting tomogram yielded a biased velocity range of 60 to 66 m/μs, instead of the true velocity range of 58 to 64 m/μs (compare Figures 6a and 6b). Note that if these corrupted estimates of radar velocity were used together with a relationship established from theoretical considerations or laboratory experiments to estimate the hydraulic conductivity field, it would also result in biased hydraulic conductivity estimates.

[54] However, by incorporating the zonation pattern (Figure 6c) to constrain the inversion of the tracer data, we find that the hydraulic conductivity estimates are centered on the background hydraulic conductivity (see Figures 6e and 6f) and that the residuals are relatively low (see Figures 6g and 6h). The correlation coefficients of 0.72 and 0.80 are close to the results of example 1 (see example 1 in Table 1) and they are more strongly related to the true hydraulic conductivity field than estimates obtained using tracer test data only (see Figure 3g, correlation coefficient of 0.093).

[55] The slopes of the empirical relationships (0.33 μs/m and 0.41 μs/m) are higher compared with the intrinsic relationship of 0.23 μs/m. Recall that fewer iterations are used in the ART inversion for data with large errors (see section 2.1), leading to smoother tomograms. The high empirical relationships indicate that a more variable hydraulic conductivity estimate improves the data fit compared with applying the intrinsic relationship directly to the tomogram. This finding illustrates that optimal petrophysical relationships in the field are dependent on measurement errors as well as the underlying physics.

[56] This example highlights the advantage of including radar and tracer data in the inversion even if the radar data set has relatively large errors. We conclude that although the radar data acquisition errors considered in this example lead to smoothing and bias, they do not create any significant bias or inversion artifacts in the resulting hydraulic conductivity estimates.

3.5. Example 5: Effects of Borehole Deviations

[57] In this last example, we consider the effect of a 2% deviation of the right borehole, while assuming that both boreholes are vertical (see example 5 in Table 1). On the basis of analyses of borehole deviation logs at hydrogeological study sites, boreholes are frequently deviated by 2% or more.

[58] It is well established that unaccounted for borehole deviations lead to tomograms that are severely distorted [*Peterson*, 2001], as is seen in the high-velocity region at the bottom of the tomogram shown in Figure 7b. Borehole deviation logs are often, but not always, collected to circumvent such inversion errors. The resulting zonation pattern obtained using the tomogram corrupted by borehole deviation errors are shown in Figure 7c. When we use these distorted tomograms within the hydrogeological inversion, we find that both the nonstationary (Figure 7e) and the

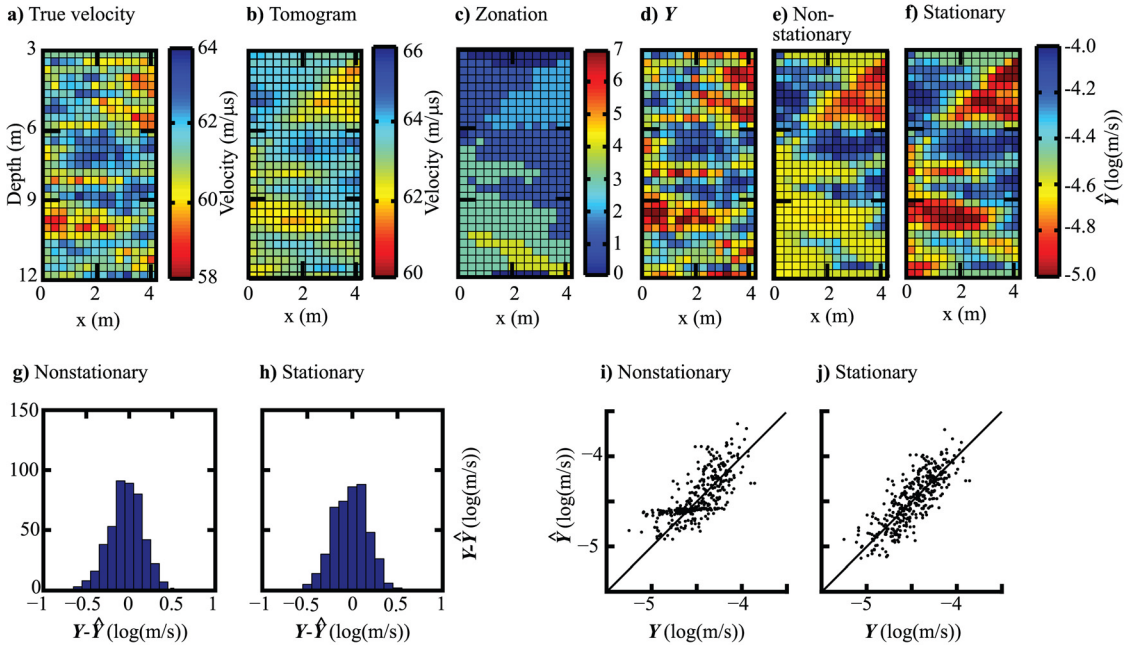

Figure 6. Results from example 4 where data acquisition errors are nonnegligable, the intrinsic correlation coefficient is 0.99, and the intrinsic relationship is stationary (example 4 in Table 1). (a) True velocity model, (b) tomogram, (c) tomographic zones used in the nonstationary inversion, (d) true hydraulic conductivity field, (e) hydraulic conductivity estimate from nonstationary inversion, (f) hydraulic conductivity estimate from stationary inversion, (g) histogram of residuals of true and estimated hydraulic conductivity field from nonstationary inversion, (h) histogram of residuals of true and estimated hydraulic conductivity field from stationary inversion, (i) scatterplot of true and estimated hydraulic conductivity field from nonstationary inversion, and (j) scatterplot of true and estimated hydraulic conductivity field from stationary inversion.

stationary hydraulic conductivity estimates (Figure 7f) are overly smooth, as is revealed by both the residuals (Figures 7g and 7h) and the scatterplots (Figures 7i and 7j). The correlation coefficients are 0.36 and 0.45, respectively. The slopes of the empirical relationships (0.053 μs/m and 0.11 μs/m, respectively) do not represent the intrinsic relationship (0.23 μs/m).

[59] As expected, borehole deviations have a large impact on the hydraulic conductivity estimates. It is therefore essential to collect borehole deviation logs along with high-resolution tomographic data sets to avoid a potentially large estimation bias. In this example, using a simple hydrogeological inversion of the tracer test data with a zonation based on borehole logs is probably preferable (see Figure 3g) to incorporation of the severely distorted zonation from the tomogram into the inversion of the tracer test data.

3.6. Evaluation Criteria Scores

[60] The criteria scores for all examples are given in the bottom of Table 1. The objective function (Cr1 in Table 1) indicates that the nonstationary inversions fit the data better than or equally good as the stationary inversions. This is expected due to the larger number of fitting parameters in the nonstationary inversion. The objective functions generally increase when decreasing the intrinsic correlation coefficients or introducing data acquisition errors.

[61] The correlation coefficients (Cr2 in Table 1) between the true and estimated hydraulic conductivity fields based on the stationary inversions are superior compared with the estimates based on the nonstationary inversions, except for the example in which two different intrinsic relationships exist (see example 2). In this example, the nonstationary inversion performs better. The stationary inversions are less influenced by three-dimensional heterogeneity as discussed in section 3.1. The residuals of the estimated hydraulic conductivity fields (Cr3 in Table 1) are rather small, and the stationary inversions have the lowest residuals for the examples where the intrinsic relationship is stationary.

[62] Finally, we note that the empirical relationships (Cr4 in Table 1) provide a reasonable estimate of the intrinsic relationship if the correlation coefficient is high (i.e., $\rho(Y, V) > 0.5$) and data acquisition errors are small. However, data acquisition errors typically yield higher slopes of the empirical relationships to compensate for the resulting tomograms being too smooth if data of low quality are used. On the other hand, if the tomogram is severely distorted, the empirical relationship is close to zero because the estimated zones are basically not revealing any hydrogeological information. Therefore empirical relationships close to zero might indicate that no intrinsic relationship exists or that the quality of the tomogram is too low to reveal the intrinsic relationship.

[63] The results presented in this work indicate what could be obtained in a real field setting for a given intrinsic relationship and radar data acquisition errors. However, we note that we disregard many other sources of error. For

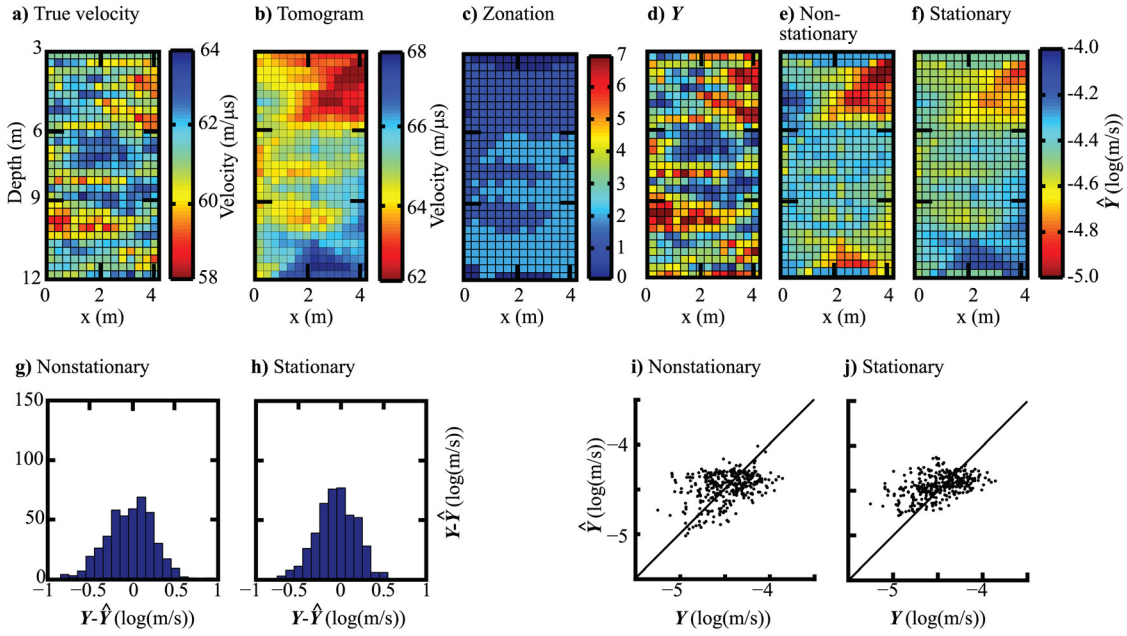

Figure 7. Results from example 5 where data acquisition errors are small except for a 2% error in the deviation of the right borehole, the intrinsic correlation coefficient is 0.99, and the intrinsic relationship is stationary (example 5 in Table 1). (a) True velocity model, (b) tomogram, (c) tomographic zones used in the nonstationary inversion, (d) true hydraulic conductivity field, (e) hydraulic conductivity estimate from nonstationary inversion, (f) hydraulic conductivity estimate from stationary inversion, (g) residuals of true and estimated hydraulic conductivity field from nonstationary inversion, (h) residuals of true and estimated hydraulic conductivity field from stationary inversion, (i) scatterplot of true and estimated hydraulic conductivity field from nonstationary inversion, and (j) scatterplot of true and estimated hydraulic conductivity field from stationary inversion.

example, we assume a linear intrinsic relationship, which is not physically based; we neglect hydrogeological features smaller than the resolution of the tomograms; and we disregard effects of the ray approximation, i.e., we assume that there is no loss in resolution due to the finite frequency content of radar signals (note that such a potentially considerable resolution loss can be approximated by Fresnel zone tomography [*Day-Lewis et al.*, 2005]). The positions of the boreholes in our examples are close to ideal, i.e., larger horizontal offsets between the boreholes or less angular coverage would degrade the resulting models compared to what is presented here. Moreover, the errors in the hydrogeological data acquisition are assumed to be small, we assume a constant porosity, and we assume that the test design is perfectly known. Nonetheless, we feel that these synthetic case studies give an indication of both the benefits and limitations of including geophysical tomographic data when inverting tracer test data to estimate a hydraulic conductivity field. The results could also be used to guide the design of geophysical cross-hole experiments (e.g., what error sources to minimize) and to provide insights into the expected worth of the resulting tomograms for hydrogeological characterization.

4. Discussion and Conclusions

[64] Our methodology uses the internal velocity variability of zones defined by tomograms to constrain the set of possible hydraulic conductivity models in a hydrogeological inverse problem, which we solve using tracer test data. Our methodology does not assume that the parameters in the petrophysical relationship are known a priori, nor do we assume that the petrophysical relationships are stationary. However, our method does rely on the existence of a relatively strong relationship, which may not exist at some sites. Our methodology simultaneously yields hydraulic conductivity estimates as well as the empirical relationship between radar velocity and hydraulic conductivity. Our main findings from synthetic models with different intrinsic correlation coefficients and radar data acquisition errors can be summarized as follows.

[65] 1. Given an intrinsic correlation coefficient between radar velocity and hydraulic conductivity of 0.5 or higher and small radar data acquisition errors, the estimated hydraulic conductivity fields derived from hydrogeological inversion using constraints from geophysical tomograms are more strongly correlated with the true hydraulic conductivity field than estimates obtained using tracer test data only.

[66] 2. We can accurately estimate the hydraulic conductivity field ($\rho(\hat{Y}, Y) > 0.8$) if a strong and stationary intrinsic relationship (correlation coefficient $\rho(Y, V) > 0.8$) exists and the geophysical data acquisition errors are very small. Furthermore, using the nonstationary inversion approach, each zone can have a different intrinsic relationship.

[67] 3. We can obtain a useful estimate the effective hydraulic conductivity using tracer and tomographic data, even if the intrinsic relationship is weak and geophysical data acquisition errors are relatively large (see criterion 3 in Table 1).

[68] 4. Geophysical data acquisition errors significantly decrease the correlation coefficient between the hydraulic conductivity estimates and the true hydraulic conductivity field (e.g., half of the correlation is lost if we have an unknown borehole deviation of 2% (example 5) compared to the case in which only very small errors are introduced (example 1)). The geophysical errors that most distort the estimates of hydraulic conductivity are borehole deviations and relative errors in the depths of the transmitters and receivers.

[69] 5. The nonstationary inversion performs better if the intrinsic relationship is nonstationary. Large deviations between the nonstationary and stationary inversion estimates indicate nonstationary intrinsic relationships or three-dimensional heterogeneity.

[70] In practice, we should realize the limitations of hydraulic conductivity estimates that are based on tomograms. For example, relationships between radar velocity and hydraulic conductivity are site-specific and may not exist at all at some sites. Despite the difficulty in estimating data errors and uncertainties in petrophysical relationships (both of which are significant problems in real field applications) this study suggests that tomographic information may be used with tracer test data to improve the estimates of hydraulic conductivity over conventional approaches. By using zonation information offered by the tomograms, the proposed inversion methodology helps to overcome some of the common obstacles associated with tomographic data.

[71] **Acknowledgments.** This research was carried out while the first author was visiting the Earth Sciences Division (ESD), Lawrence Berkeley National Laboratory, Berkeley, California. We want to thank ESD director Gudmundur (Bo) Bodvarsson for making this stay possible and John Peterson for use of and assistance with his ART algorithm. This work was supported, in part, by the Office of Science Environmental Remediation Science Division of the U.S. Department of Energy under contract DE-AC03-76SF00098. Comments from the Associate Editor and three anonymous reviewers have significantly helped to improve the clarity of this paper.

References

Alumbaugh, D., P. Y. Chang, L. Paprocki, J. R. Brainard, R. J. Glass, and C. A. Rautman (2002), Estimating moisture contents in the vadose zone using cross-borehole ground penetrating radar: A study of accuracy and repeatability, *Water Resour. Res.*, *38*(12), 1309, doi:10.1029/2001WR000754.

Annan, A. P. (2005), GPR methods for hydrogeological studies, in *Hydrogeophysics*, edited by Y. Rubin and S. Hubbard, chap. 7, pp. 185–214, Springer, New York.

Binley, A., G. Cassiani, R. Middleton, and P. Winship (2002), Vadose zone flow model parameterisation using cross-borehole radar and resistivity imaging, *J. Hydrol.*, *267*(3–4), 147–159.

Carrera, J., and S. P. Neuman (1986a), Estimation of aquifer parameters under transient and steady state conditions: 1. Maximum likelihood method incorporating prior information, *Water Resour. Res.*, *22*(2), 199–210.

Carrera, J., and S. P. Neuman (1986b), Estimation of aquifer parameters under transient and steady state conditions: 2. Uniqueness, stability, and solution algorithms, *Water Resour. Res.*, *22*(2), 211–227.

Carrera, J., and S. P. Neuman (1986c), Estimation of aquifer parameters under transient and steady state conditions: 3. Application to synthetic and field data, *Water Resour. Res.*, *22*(2), 228–242.

Chen, J., S. Hubbard, and Y. Rubin (2001), Estimating the hydraulic conductivity at the South Oyster Site from geophysical tomographic data using Bayesian techniques based on the normal linear regression model, *Water Resour. Res.*, *37*(6), 1603–1613.

Chen, J., S. Hubbard, Y. Rubin, C. Murray, and E. Roden (2004), Geochemical characterization using geophysical data and Markov chain Monte Carlo methods: A case study at the South Oyster Bacterial Transport Site in Virginia, *Water Resour. Res.*, *40*, W12412, doi:10.1029/2003WR002883.

Copty, N., Y. Rubin, and G. Mavko (1993), Geophysical-hydrological identification of field permeabilities through Bayesian updating, *Water Resour. Res.*, *29*(8), 2813–2825.

Daily, W., A. Ramirez, D. LaBrecque, and J. Nitao (1992), Electrical resistivity tomography of vadose water movement, *Water Resour. Res.*, *28*(5), 1429–1442.

Day-Lewis, F. D., and J. W. Lane Jr. (2004), Assessing the resolution-dependent utility of tomograms for geostatistics, *Geophys. Res. Lett.*, *31*, L07503, doi:10.1029/2004GL019617.

Day-Lewis, F. D., J. W. Lane, J. M. Harris, and S. M. Gorelick (2003), Time-lapse imaging of saline-tracer transport in fractured rock using difference-attenuation radar tomography, *Water Resour. Res.*, *39*(10), 1290, doi:10.1029/2002WR001722.

Day-Lewis, F. D., K. Singha, and A. M. Binley (2005), Applying petrophysical models to radar travel time and electrical resistivity tomograms: Resolution-dependent limitations, *J. Geophys. Res.*, *110*, B08206, doi:10.1029/2004JB003569.

Deutsch, C. V., and A. G. Journel (1998), *GSLIB: A Geostatistical Software Library and User's Guide*, 2nd ed., Oxford Univ. Press, New York.

Eppstein, M. J., and D. E. Dougherty (1998), Optimal 3-D traveltime tomography, *Geophysics*, *63*(3), 1053–1061.

Finsterle, S. (1999), iTOUGH2 user's guide, *Rep. LBNL-40040*, Lawrence Berkeley Natl. Lab., Berkeley, Calif.

Gritto, R., V. A. Korneev, T. M. Daley, M. Feighner, E. L. Majer, and J. E. Peterson (2004), Surface-to-tunnel seismic tomography studies at Yucca Mountain, Nevada, *J. Geophys. Res.*, *109*, B03310, doi:10.1029/2002JB002036.

Hoeksema, R. J., and P. K. Kitanidis (1984), An application of the geostatistical approach to the inverse problem in two-dimensional groundwater modeling, *Water Resour. Res.*, *20*(7), 1003–1020.

Hubbard, S. S., Y. Rubin, and E. Majer (1999), Spatial correlation structure estimation using geophysical and hydro-geological data, *Water Resour. Res.*, *35*(6), 1809–1825.

Hubbard, S. S., J. Chen, J. Peterson, E. L. Mayer, K. H. Williams, D. J. Swift, B. Mailloux, and Y. Rubin (2001), Hydrogeological characterization of the South Oyster Bacterial Transport Site using geophysical data, *Water Resour. Res.*, *37*(10), 2431–2456.

Hyndman, D. W., and S. M. Gorelick (1996), Estimating lithological and transport properties in three dimensions using seismic and tracer data: The Kesterson aquifer, *Water Resour. Res.*, *32*(9), 2659–2670.

Hyndman, D. W., and J. M. Harris (1996), Traveltime inversion for the geometry of aquifer lithologies, *Geophysics*, *61*(6), 1728–1737.

Hyndman, D. W., J. M. Harris, and S. M. Gorelick (1994), Coupled seismic and tracer test inversion for aquifer property characterization, *Water Resour. Res.*, *30*(7), 1965–1977.

Hyndman, D. W., J. R. Harris, and S. M. Gorelick (2000), Inferring the relation between seismic slowness and hydraulic conductivity in heterogeneous aquifers, *Water Resour. Res.*, *36*(8), 2121–2132.

Irving, J. D., and R. Knight (2005), Effect of antennas on velocity estimates obtained from crosshole GPR data, *Geophysics*, *70*(5), K39–K42, doi:10.1190/1.2049349.

Kowalsky, M. B., S. Finsterle, and Y. Rubin (2004), Estimating flow parameter distributions using ground-penetrating radar and hydrological measurements during transient flow in the vadose zone, *Adv. Water Resour.*, *27*(6), 583–599.

Kowalsky, M., S. Finsterle, J. Peterson, S. Hubbard, Y. Rubin, E. Majer, A. Ward, and G. Gee (2005), Estimation of field-scale soil hydraulic parameters and dielectric parameters through joint inversion of GPR and hydrological data, *Water Resour. Res.*, *41*, W11425, doi:10.1029/2005WR004237.

Lesmes, D. P., and S. Friedman (2005), Relationships between the electrical and hydrogeological properties of rocks and soils, in *Hydrogeophysics*, edited by Y. Rubin and S. Hubbard, chap. 4, pp. 87–128, Springer, New York.

Marquardt, D. W. (1963), An algorithm for least squares estimation of nonlinear parameters, *SIAM J. Appl. Math.*, *11*, 431–441.

McKenna, S. A., and E. P. Poeter (1995), Field example of data fusion in site characterization, *Water Resour. Res.*, *31*(12), 3229–3240.

McLaughlin, D., and L. R. Townley (1996), A reassessment of the groundwater inverse problem, *Water Resour. Res.*, *32*(5), 1131–1161.

Menke, W. (1984), *Geophysical Data Analysis: Discrete Inverse Theory*, Springer, New York.

Moysey, S., K. Singha, and R. Knight (2005), A framework for inferring field-scale rock physics relationships through numerical simulation, *Geophys. Res. Lett.*, *32*, L08304, doi:10.1029/2004GL022152.

Paige, C. C., and M. A. Saunders (1982), LSQR: An algorithm for sparse linear equations and sparse least squares, *Trans. Math. Software*, *8*(1), 43–71.

Peterson, J. E. (1986), The application of algebraic reconstruction techniques to geophysical problems, Ph.D. thesis, Univ. of Calif., Berkeley, Calif.

Peterson, J. E. (2001), Pre-inversion processing and analysis of tomographic radar data, *J. Environ. Eng. Geophys.*, *6*(1), 1–18.

Peterson, J. E., B. N. Paulsson, and T. V. McEvilly (1985), Applications of algebraic reconstruction techniques to crosshole seismic data, *Geophysics*, *50*, 1566–1580.

Prasad, M. (2003), Velocity-permeability relations within hydraulic units, *Geophysics*, *68*(1), 108–117.

Pride, S. R. (2005), Relationships between seismic and hydrological properties, in *Hydrogeophysics*, edited by Y. Rubin and S. Hubbard, chap. 3, pp. 253–290, Springer, New York.

Pruess, K., C. Oldenburg, and G. Moridis (1999), TOUGH2 user's guide, version 2.0, *Rep. LBNL-43134*, Lawrence Berkeley Natl. Lab., Berkeley, Calif.

Rector, J. W., and J. K. Washbourne (1994), Characterization of resolution and uniqueness in crosswell direct-arrival traveltime tomography using the Fourier projection slice theorem, *Geophysics*, *59*(11), 1642–1649.

Revil, A., and L. M. Cathles (1999), Permeability of shaly sands, *Water Resour. Res.*, *35*(3), 651–662.

Rucker, D. F., and T. P. A. Ferré (2004), Correcting water content measurement errors associated with critically refracted first arrivals on zero offset profiling borehole ground penetrating radar profiles, *Vadose Zone J.*, *3*, 278–287.

Scheibe, T. D., and Y. J. Chien (2003), An evaluation of conditioning data for solute transport prediction, *Ground Water*, *41*(2), 128–141.

Schuster, G. T. (1996), Resolution limits for crosswell migration and traveltime tomography, *Geophys. J. Int.*, *127*(2), 427–440.

Slater, L. D., A. Binley, and D. Brown (1997), Electrical imaging of fractures using ground-water salinity change, *Ground Water*, *35*(3), 436–442.

Slater, L., A. Binley, R. Versteeg, G. Cassiani, and R. Birken (2002), A 3D ERT study of solute transport in a large experimental tank, *J. Appl. Geophys.*, *49*(4), 211–229.

Spitzer, F. (1976), *Principles of Random Walk*, 2nd ed., Springer, New York.

Tronicke, J., K. Holliger, W. Barrash, and M. D. Knoll (2004), Multivariate analysis of cross-hole georadar velocity and attenuation tomograms for aquifer zonation, *Water Resour. Res.*, *40*, W01519, doi:10.1029/2003WR002031.

S. Finsterle and S. Hubbard, Earth Sciences Division, Lawrence Berkeley National Laboratory, MS 90-1116, 1 Cyclotron Road, Berkeley, CA 94720, USA.

N. Linde, CEREGE, CNRS, Université Paul Cézanne, Europôle Méditerranéen de l'Arbois, BP 80, F-13545 Aix-en-Provence, France. (linde@cerege.fr)